Novel evaluation method of neutron reflectivity data applied to stimulus-responsive polymer brushes

Jianming Zhang,[a] Tommy Nylander,[b] Richard A. Campbell,[b] Adrian R. Rennie,[c] Stefan Zauscher[a] and Per Linse[b]

Received 27th September 2007, Accepted 10th December 2007
First published as an Advance Article on the web 8th January 2008
DOI: 10.1039/b714911e

Neutron reflectivity (NR) measurements have been performed on stimulus-responsive polymer brushes containing *N*-isopropylacrylamide (NIPAAM) at different temperatures and contrasts using two different brush samples of roughly the same grafting density and layer thickness. The NR data were analyzed using a novel method employing polymer density profiles predicted from lattice mean-field theory augmented with a polymer model to describe polymer solubility that decreases with increasing temperature. The predicted density profiles at the different temperatures were self-consistent with the experimentally observed profiles; hence the experimental data lend credibility to the theory. We found that the brush thickness decreased from 220 to 160 nm and the polymer volume fraction increased from 55 to 75% when increasing temperature from 293 to 328 K. The new evaluation approach involved significantly fewer independent fitting parameters than methods involving layers of uniform densities. Furthermore, the approach can straightforwardly be extended to analyze neutron reflectivity data of grafted, weakly charged polymers that display pH-sensitive behaviour and also to block copolymers and to surfaces with adsorbed polymers. We propose that such accurate model calculations provide a tool to interpret results from NR experiments more effectively and design neutron reflectivity experiments for optimal outcome.

1 Introduction

Polymer brushes with triggerable phase transition behaviour, such as poly(*N*-isopropylacrylamide) (pNIPAAM) brushes, can be exploited in sensing and actuation devices on the nanoscale with potential applications for protein affinity separations,[1,2] sensing,[3] and in microfluidics.[4] A number of methods have been used to characterize the phase transition behaviour and conformation of pNIPAAM on surfaces, including surface plasmon resonance (SPR),[5] atomic force microscopy (AFM),[6–12] neutron reflectivity (NR),[13–15] quartz crystal microbalance with dissipation monitoring (QCM-D),[16–18] and ellipsometry.[19] The consensus of these measurements is that end-grafted pNIPAAM brush undergoes a large conformational collapse in response to an increase in temperature. Although this unusual temperature dependence of pNIPAAM brushes can be interpreted in the context of a reverse solubility behaviour, a detailed understanding of the changes in conformation and hydration of pNIPAAM-containing homopolymer and copolymer brushes on the sub-molecular level is still largely missing. Furthermore the existence of conformational hysteresis and intermediate conformational states, found for single pNIPAAM homopolymer chains,[20,21] remains unexplored for pNIPAAM brushes. This information is, however, essential for the synthesis and the design of stimulus-responsive brushes for sensing and actuation applications. For example, the persistence of irreversibly folded polymer brush structures on patterned surfaces (impeding the regeneration of original brush conformation) may significantly affect their usefulness. Thus, insight into polymer brush conformation on the sub-molecular level allows rational brush design and guides brush synthesis.

Neutron reflectivity offers a powerful tool to determine segment density profiles in grafted polymer layers at the sub-molecular level.[22] Although NR has been applied recently to study the conformational behaviour of pNIPAAM homopolymer brushes as a function of molecular weight and solvent conditions,[13–15] the effects of molecular architecture (copolymerization) have not yet been studied.

In this paper, we determine the structure of poly-(*N*-isopropylacrylamide-*co*-acrylic acid) (poly-(NIPAAM-*co*-AA)) random copolymer brushes using NR at different temperatures in different solvent contrasts. The interpretation of the NR data was performed by using two different approaches: (i) a simple model that uses a single homogeneous layer[23,24] and (ii) a novel approach utilizing polymer brush theory. In the conventional approach, a polymer brush is represented by one uniform layer (or sometimes several layers) of constant polymer density, and to improve the representation of the experimental data, the edges of the layer(s) are often smoothed using a Gaussian function, the width of which is referred to as a roughness parameter. In the new approach, polymer brush segment density profiles obtained from polymer theory are used to represent the experimental data. Specifically, we have used a molecular-based lattice mean-field theory augmented with an extension that enables a physical description of the reverse solubility displayed by pNIPAAM to

[a]*Department of Mechanical Engineering and Materials Science, Duke University, 144 Hudson Hall, Durham, NC, 27708, USA*
[b]*Physical Chemistry 1, Center for Chemistry and Chemical Engineering, Lund University, Box 124, SE-221 00 Lund, Sweden*
[c]*Department of Physics, Uppsala University, Box 530, SE-751 21 Uppsala, Sweden*

model segment density profiles. Necessary model parameters describing the copolymer–water interaction were determined independently from solubility data. Our global representation of the NR brush data (i) required only three fitting parameters, which is considerably fewer than the six required by the conventional layer approach, and (ii) captures self-consistently the thermal response of the brush. Furthermore, the good description of the experimental data provided by our approach lends credibility to the polymer theory we apply.

Over a number of years, there have been various studies of the molecular density profiles in brushes and other bound polymer layers using NR. Beside the homogeneous layer model, Gaussian, exponential, and parabolic functions based on scaling theories have been used to analyze the reflectivity profiles.[25–28]

Thermoresponsive polymer brushes are ideal samples for the proof-of-principle demonstration of our novel approach of modelling NR data. The fact that they can be stimulated into different hydration states while maintaining a fixed mass of polymer on the surface provides a self-consistent test of the method. Our approach of incorporating a realistic polymer brush description directly into the representation of NR data is general in the sense that (i) any suitable polymer brush theory can be employed and (ii) it can be applied to grafted polyelectrolytes and block copolymers, and to surfaces with adsorbed polymers.

2 Experimental

2.1 Material

Sodium acrylate (NaAA, 99%) monomer, *N*-isopropylacrylamide (NIPAAM, 97%) monomer, and methanol (MeOH, 99.9%) were obtained from Sigma-Aldrich (Milwaukee, WI). NIPAAM was purified by recrystallisation from toluene–hexane before use. Other chemicals were used without further purification. MQ-Grade water (Millipore purification unit, 18 MΩ cm) was used in all experiments. To adjust the pH, small amounts of 0.1 M HCl or 0.1 M NaOH were added. The synthesis of the ATRP initiator, [11-(2-bromo-2-methyl)propionyloxy]undecyl trichlorosilane, has been described elsewhere.[29]

The silicon substrates were oxide layers on the 111 faces of single crystals of silicon (50 × 50 × 10 mm). These were first rinsed in MQ-grade water and then cleaned in a solution consisting of water, sulfuric acid (98%), and hydrogen peroxide solution (27.5% in water) mixed in a volume ratio of 5 : 4 : 1 respectively at 80 °C for 40 minutes. The substrates were removed from the cleaning solution and allowed to cool for a few minutes before being quenched by immersion in MQ-grade water. Finally, the substrates were plasma cleaned in a stream of oxygen and exposed to ultraviolet light for 30 minutes.

2.2 Sample preparation

Prior to use, all solutions and scintillation vials were thoroughly flushed with dry nitrogen gas to remove oxygen. A self-assembled monolayer (SAM) of the initiator was obtained on the silicon substrate by immersing a cleaned substrate into a dilute (1 mM) anhydrous toluene solution of the initiator for 30 minutes. After removing the substrate from the solution, its surface was sequentially rinsed with anhydrous toluene, ethanol, and MQ-grade water, and finally dried in a stream of dry nitrogen.

The polymerization reactions were initiated on the silicon substrates immediately after SAM deposition. A polymerization solution was prepared in a nitrogen atmosphere by injecting 100 ml of 0.1 M degassed phosphate buffered saline (PBS) solution at pH 7.4 into a nitrogen-flushed scintillation vial containing a 15.39 g (136 mmol) NIPAAM monomer and 1.17 g (12.4 mmol) NaAA which resulted in 14 wt% monomer solution with a fixed molar monomer feed ratio of NIPAAM to NaAA of 11 : 1. The polymerization solution was then transferred into nitrogen-flushed scintillation vials containing the initiator-functionalized substrates. The poly-(NIPAAM-*co*-AA) copolymer brushes were polymerized for 2 h without stirring at 293–298 K under nitrogen. The polymerization temperature was kept below the lower critical solution temperature of 305 K of pNIPAAM. Substrates were then removed from the polymerization solution and immediately rinsed with copious amounts of MQ-grade water and MeOH to remove all traces of the polymerization solution, and they were subsequently dried under a stream of nitrogen. Physically absorbed copolymer was removed from the silicon oxide substrate by rigorous rinsing with water and MeOH. In this study, we only consider systems at pH 4.0, where the acrylate is protonated to uncharged acrylic acid.

2.3 Cloud-point measurements

The phase behaviour of aqueous poly-(NIPAAM-*co*-AA) solutions was characterized by monitoring the optical density at 350 nm as a function of temperature using a UV–visible spectrophotometer equipped with a multicell thermoelectric temperature controller (Cary 300Bio; Varian Instruments). The phase transition temperatures of poly-(NIPAAM-*co*-AA) at different solution concentrations were determined in buffer at pH 4.0 (0.2 M potassium hydrogen phthalate buffer). The reversibility of the phase transition behaviour was examined by first heating a poly-(NIPAAM-*co*-AA) solution, from 303 to 318 K at a rate of 0.5 K min^{-1}, and then cooling the solution to 303 K at the same rate. Fig. 1 shows the normalized absorbance as a function of temperature for different polymer concentrations. It can be seen that the transition temperature decreases with increasing concentration from 311 K at 0.1 g per 100 ml solution to 306 K at 5 g per 100 ml.

2.4 Neutron reflectivity experiments

Generally, NR data are collected by simple measurements of the specular reflection of a neutron beam from a planar substrate.

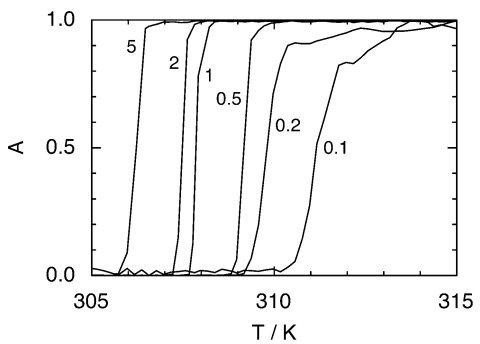

Fig. 1 Normalized absorbance (*A*) *versus* the temperature (*T*) for the random copolymer at pH 4.0 at indicated polymer concentrations (g per 100 ml solution).

The reflected intensity depends on the average neutron refractive index profile normal to the interface. This refractive index profile can then be related to the composition profile by using the known scattering length of atomic nuclei.[30,31] The experimentally measured reflectivity, R, is typically plotted as a function of the momentum transfer, q, that is defined as $q = (4\pi/\lambda)\sin\theta$ with λ denoting the wavelength of the neutron and θ the grazing angle of incidence. This expression shows that the reflectivity $R(q)$ can be obtained by either measuring at different wavelengths λ or angles θ. The neutron refractive index, n, for a material is given by $n = 1 - \lambda^2\rho/(2\pi)$ with $\rho = \Sigma_i b_i/V$, where b_i is the nuclear scattering length of nucleus i that appears in the total volume V. The significantly different scattering length of the two hydrogen isotopes ^{1}H and ^{2}H (D, deuterium) can be exploited to provide different contrasts in otherwise chemically identical materials.

The NR measurements reported here were conducted at two different neutron sources: (i) the NG7 neutron reflectometer[32] at the NIST Center for Neutron Research (NCNR) at the National Institute of Standards and Technology in Gaithersburg, Maryland, USA, and (ii) the D17 neutron reflectometer[33] at the Institut Laue-Langevin (ILL) in Grenoble, France. The incident wavelength of the NCNR instrument was 4.75 Å and the data at different momentum transfer were collected by changing the incident beam angle and the detector angle in a sequential scan, while neutron wavelengths from 2 to 19 Å were used in the experiments at ILL using a time-of-flight mode with two different incident angles to provide a range of momentum transfer from 0.006 to 0.2 Å^{-1}. At NCNR the wavelength resolution dq/q is about 2%, but slit widths that define the angular resolution and data binning were chosen to provide an overall resolution of about 5%. At ILL the beam is pulsed with a chopper system and the opening was chosen to provide a resolution in dλ/λ of about 2%. The reflectivity data obtained at ILL were binned to reduce the statistical uncertainty, which increased the resolution dq/q to about 3%.

Reflectivity data from the polymer brush layers were collected over a range of temperatures from 298 to 330 K (NCNR) and from 293 to 333 K (ILL) at pH 4.0 in different solvent contrasts: deuterated water (D_2O), hydrogenated water (H_2O), and a mixture of 37.9% (by volume) D_2O in H_2O, designed to be matched in scattering length density to silicon (contrast matched silicon; cmSi). Independent measurements on the same sample in different scattering contrasts allow determination of the composition and thickness of the grafted layers. Two distinct but similarly prepared surfaces with grafted polymer were used in the measurements at NCNR and ILL. The samples measured at NCNR had a more heterogeneous grafting density; the work formed part of a broader study on block copolymers. The samples measured at ILL had lower polydispersity, and the grafted polymer formed sharper layers with clearer fringes in the reflectivity profiles when in a collapsed state above the lower critical solution temperature (LCST).

3. Model

Theoretically predicted brush segment density profiles were used in the analysis of the NR data. The model calculations involve two sequential parts: (i) a determination of model parameters describing the interactions in an aqueous polymer solution obtained by fitting predicted binodal curves to the experimentally determined phase behaviour, and (ii) a prediction of polymer brush density profiles to be used in the evaluation of the NR data. An important issue for the analysis of the NR results is that the *same* underlying model should be used in the evaluation of the data at *all* experimental conditions. Hence, the model employed here should be able to describe thermo-responsive polymer systems at various temperatures.

Although NR measurements were performed on stimulus-responsive random copolymer brushes, we have, for simplicity, modelled these brushes as a homopolymer with solution properties that reflect those of the two monomers. Although it is straightforward to handle random and block copolymers as well as mixtures of polymers with the present approach, a larger set of parameters describing the interaction would be needed, which would require a significantly more extensive set of solubility measurements.

3.1 Polymer solution model

The classical Flory–Huggins theory for homogeneous polymer solutions,[34] extended with a polymer model containing internal degrees of freedom by Karlström,[35] was used to describe the polymer solutions. This extension was originally developed to model aqueous solution of poly(ethylene oxide) (PEO), using a physical model. In common with pNIPAAM, aqueous solutions of PEO display a reverse solubility, leading to a phase separation at increasing temperature. While we use the same formalism, the parameters entering the polymer model are obtained here from fits to experimental data rather than determined using quantum mechanical arguments.

The Flory–Huggins theory is a lattice theory in which space is divided into cells, each containing one polymer segment or solvent. The division into cells facilitates the enumerations of the chain configurations and hence the evaluation of the entropy of the system. Only nearest-neighbour interactions are considered, and they are described by a so-called χ-parameter. A positive $\chi_{xx'}$ implies that the interaction between components x and x' is more repulsive than the average of the x–x and x'–x' interactions, a component being a polymer or solvent. A mean-field approximation is applied, neglecting all density fluctuations in a phase, and the polymer is assumed to be fully flexible.

The basis of Karlström's polymer model for describing polymer solutions with reverse solubility behaviour is that a polymer segment can appear in one of two different states. Generally, a segment of type A (referred to as species A) in state B is characterized by its internal energy U_{AB} and degeneration g_{AB}, and its interactions with species A′ in state B′ by $\chi_{BB'}$. The more hydrophilic state has a low internal energy and a low statistical weight, whereas the more hydrophobic state has a higher internal energy and a higher statistical weight. At low temperature the former state dominates, and thus a more favourable polymer–water interaction is obtained, whereas at elevated temperatures, the latter state becomes progressively more important, resulting in a more unfavourable polymer–water interaction. On the basis of the mixing free energy of polymer solutions, a determination can be made whether a given polymer solution is thermodynamically stable or if it separates into two coexisting phases.[36]

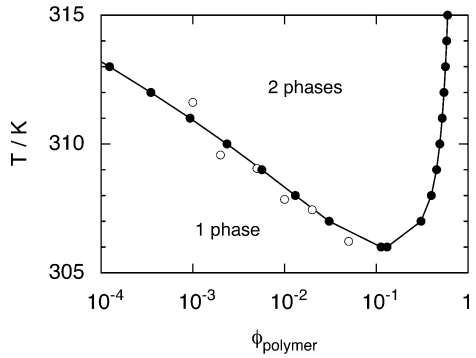

Fig. 2 Experimental cloud-point curve for the random copolymer taken from the inflection points of the absorbance data in Fig. 1 (open symbols) and calculated binodal curve obtained from a lattice mean-field theory (filled symbols), plotted on a semi-logarithmic scale. The solvent and the polymer have been assumed to have the same density; other model parameters are listed in Table 1 and $r_{polymer} = 1000$.

Fig. 2 shows (i) the experimental cloud-point curve obtained from the inflection points of the UV–vis absorption measurements shown in Fig. 1 and (ii) a fitted binodal curve plotted as a function of the logarithm of the polymer volume fraction, $\phi_{polymer}$. In addition to the degree of polymerization, which was set to $r_{polymer} = 1000$ (for large $r_{polymer}$ the phase diagram is insensitive to the precise vale of $r_{polymer}$), five other non-trivial parameters are involved to describe the polymer solution behaviour. Excellent agreement between the experimental data and fitted curve is achieved with the values listed in Table 1. Moreover, a LCST of $T^* \approx 306$ K is predicted.

3.2 Polymer brush model

The lattice mean-field theory, developed by Scheutjens and Fleer for heterogeneous polymer systems[37,38] and extended with Karlström's polymer model by Linse and Björling,[39,40] was used to model polymer brushes. This polymer theory is very general and able to describe, *e.g.*, self-association of polymers into various morphologies, polymer adsorption, and polymer-mediated forces between surfaces.[38]

The Scheutjens–Fleer theory can be viewed as an extension of the Flory–Huggins theory. In the current application, the solution near the surface is divided into layers parallel to the planar surface. The thickness of the layers corresponds to the size of a polymer segment. Within each layer, the random-mixing approximation is applied, and hence all lattice sites in a layer are equivalent. However, density gradients are allowed to develop perpendicular to the surface. The equilibrium distribution of the polymer is obtained, again, by minimization of the free energy of the system.[39] The theoretical description is quite involved, but efficient numerical approaches[41] provide solutions typically within seconds on a simple computer.

In the current application, polymers are grafted on to a smooth surface with grafting density σ (number of chains per lattice length squared). In addition to the parameters determined above and given in Table 1, we need to assign values of (i) interaction parameters for the surface $\chi_{surface,B}$, (ii) the degree of polymerization $r_{polymer}$, and (iii) the polymer grafting density σ. Unfortunately, none of these are available from direct measurements. Here, we have employed values of $\chi_{surface,B}$ corresponding to a hydrophobic surface, $r_{polymer} = 1000$, and $\sigma = 0.08$, of which σ has been fitted to experimental NR data. A second fitting parameter is the factor d, converting the lattice length unit to real length. This conversion factor should be approximately one Kuhn segment, *i.e.*, the length of a few monomers. It turned out that the predicted NR curves were insensitive to the precise value of $r_{polymer}$, provided that the brush height remained the same by adjusting d. Thus, the fitting of the polymer brush using the lattice polymer theory involved two fitting parameters, *viz.* σ and d. If the grafting density could be determined by an independent method, the number of fitting parameters representing the brush would be reduced to one.

Fig. 3 displays predicted volume fraction profiles at $T = 293$ and 328 K. At the higher temperature, a collapse of the brush is observed, consistent with the phase behaviour displayed in Fig. 2. The two volume fraction profiles shown in Fig. 3 are used below to provide the real space contrast to evaluate the experimental NR data.

Table 1 Internal state parameters (U_{AB} and g_{AB}) and Flory–Huggins interaction parameters ($\chi_{BB'}$) of the theoretical model (energy in kJ mol^{-1})

Species	State	U_{AB}	g_{AB}
Water	—	0	1
Polymer	Polar	0	1
	Nonpolar	7	16

$kT\chi_{BB'}$	Polymer (polar)	Polymer (nonpolar)
Water	0.89	7.1
Polymer (polar)	—	1.35

4 Neutron reflectivity calculations

All reflectivity profiles were calculated from the structural models of the interface employing the standard optical matrix method, which has been described in detail elsewhere.[42] Two different approaches were employed to represent the polymer brush: (i) the conventional one using a homogeneous layer model and (ii) a novel one utilizing the polymer lattice mean-field theory described above. In the second approach, each lattice

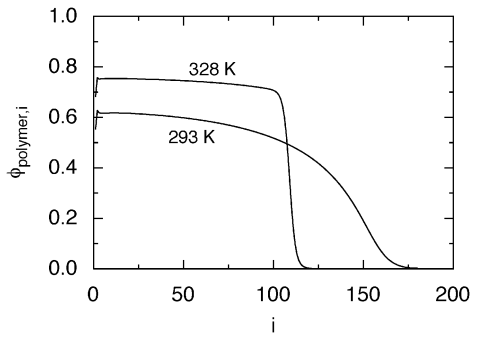

Fig. 3 Calculated polymer volume fraction $\phi_{polymer,i}$ of a polymer brush *versus* the distance i (in lattice units) from a hydrophobic surface for a polymer length $r_{polymer} = 1000$ and a grafting density $\sigma = 0.08$ at indicated temperatures.

Table 2 Scattering length densities (ρ_i) of pure components

Component	$\rho_i/10^{-6}$ Å^{-2}
Si	2.076
SiO_2	3.41
H_2O	−0.56
D_2O	6.35
Initiator	0.74
Polymer	0.57

layer of the lattice theory was treated as one optical layer with a uniform density. Generally, the scattering length density of a layer ρ was evaluated according to

$$\rho = \phi_i\rho_i + (1 - \phi_i)\rho_{\text{solvent}}, \quad (1)$$

where ϕ_i is the volume fraction of component i in the layer, ρ_i the scattering length density of component i, and ρ_{solvent} the scattering length density of the solvent. The scattering length densities used for pure components are compiled in Table 2. Since we only use the ILL data in our numerical evaluation, a single q-resolution of 3% has been applied in all calculations of reflectivity profiles.

The fitting parameters of the structural models were determined by varying the values of these parameters and visually comparing predicted and experimental reflectivity data. The uncertainties reported are based on predicted reflectivity curves displaying unacceptable fits.

5 Results

5.1 Bare surface and surface with initiator

5.1.1 Experimental neutron reflectivity data. Fig. 4 shows the experimental reflectivity data obtained at ILL for the bare Si/SiO_2 surface (top) and the Si/SiO_2/initiator surface (bottom) in D_2O, H_2O, and cmSi. As expected, a total reflection at low q occurred for D_2O as solvent, and the weakest reflection appeared in cmSi.

5.1.2 Uniform layer model. To fit the reflectivity from the bare substrate, a scattering length density model with a single uniform layer and sharp interfaces was used to represent the silicon oxide layer, sandwiched between semi-infinite silicon and solvent. In this case, the experimental NR data was fitted using a single variable, representing the thickness of the native silicon oxide layer. Excellent fits were obtained for D_2O and H_2O, but for cmSi deviations appeared at low and high q (see the three top panels of Fig. 4). A possible reason for these deviations is the small signal intensity typical for measurements in cmSi, which leads to large uncertainties when the background scattering is subtracted. This problem does not appear with other contrasts as the reflectivity is higher. The details of the fit to the oxide layer are insignificant when considering the much larger signal from the polymer brush even in cmSi. The fitted thickness of the oxide layer was 9 Å (Table 3), which is in agreement with other recent experiments.[43] Adding a roughness at the SiO_2/solvent interface did not significantly affect the fit.

For the surface with attached initiator, the silicon oxide and initiator layers were each modelled with one layer with sharp interfaces. The thickness of the silicon oxide layer was taken to be 9 Å, whereas (i) the initiator volume fraction of the initiator layer and (ii) the thickness of the initiator layer were fitted. Again, excellent fits were obtained for D_2O and H_2O, but for cmSi a significant deviation at low q appeared (see the three bottom panels of Fig. 4). We obtained an initiator volume fraction of 75% and a thickness of the initiator layer of 30 Å (Table 3). As before, a fit with a rough initiator/solvent interface did not significantly improve the fit.

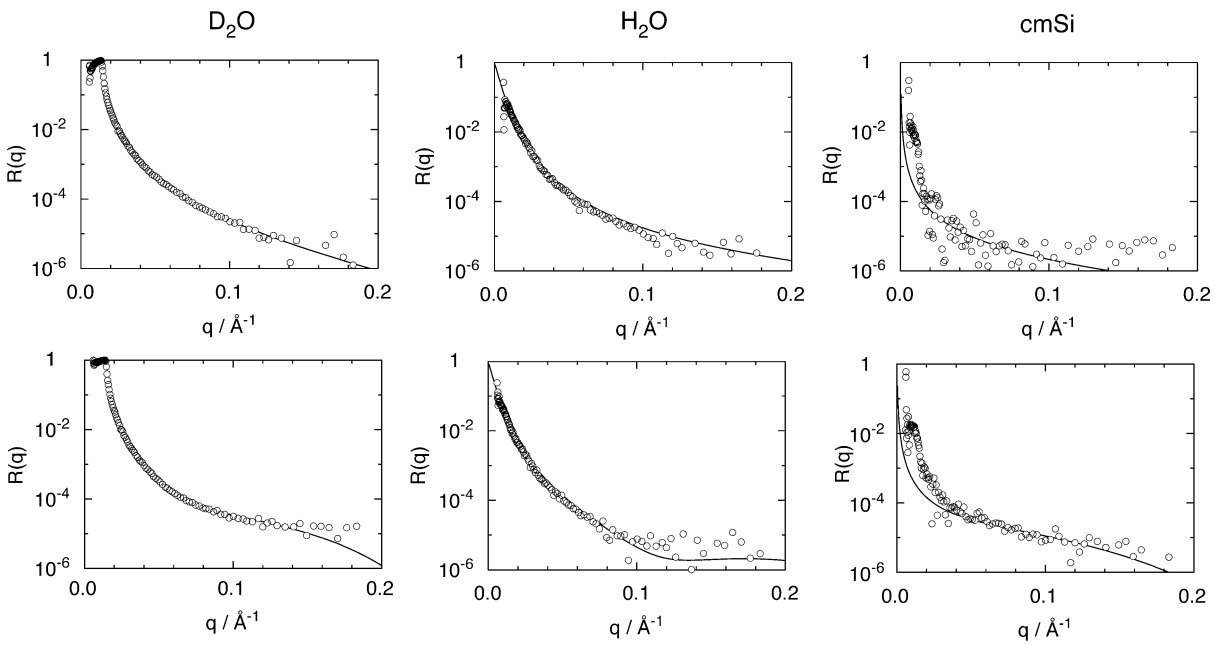

Fig. 4 Experimental reflectivity profiles obtained at ILL (symbols) and fitted reflectivity profiles using a scattering length density layer model (curves) for the bare Si/SiO_2 surface (top) and Si/SiO_2/initiator surface (bottom) in D_2O (left), H_2O (middle), and cmSi (right).

Table 3 Volume fractions (ϕ_i), thicknesses (l_i), and roughnesses (δ_i) of the uniform layer model for polymer-free systems[a]

Layer	ϕ_i	l_i/Å	δ_i/Å
Si/SiO$_2$/solvent system			
Si	1	Semi-infinite	0
SiO$_2$	1	9 ± 2^b	0
Si/SiO$_2$/initiator/solvent system			
Si	1	Semi-infinite	0
SiO$_2$	1	9	0
Initiator	0.75 ± 0.05^b	30 ± 3^b	0

[a] The scattering length density of a layer was evaluated according to eqn (1). [b] Fitted.

5.2 Surface with initiator and polymer brush

5.2.1 Experimental neutron reflectivity data. Fig. 5 shows the experimental NR data of two independently prepared brushes, measured at the two different facilities (crosses and open circles), both at high and low temperatures, and both in D_2O and in cmSi. There is a surprisingly good superposition of NR data from the two sets of measurements on samples prepared in a similar way, which validates the experimental procedures used in the reflectivity experiments. We chose to acquire the reflectivity data at ILL with higher q-resolution, although there are larger uncertainties from poorer counting statistics. An important feature in the data obtained at ILL are the fringes that appear at low q in cmSi at high temperature. Most likely this is due to a more homogeneous grafting density in the brush sample used in the ILL experiments, so the interface between the polymer and solvent was sharper. The higher q-resolution and the fringes make the ILL data more useful than the NCNR data for our fitting procedure.

We will now focus on the representation of the experimental NR data obtained at ILL by using (i) the uniform layer model and (ii) the lattice mean-field model. In both approaches, the previously obtained thicknesses of the silicon oxide and the initiator layers were used; however, for both polymer models, substantial improvements of the representations were obtained by increasing the initiator volume fraction of the initiator layer from 75% (polymer-free system) to 85% (polymer brush present). This apparent exclusion of solvent could be rationalized by a smaller solvation of the initiator layer when it is coated with a polymer layer compared to when it is in direct contact with the solvent.

5.2.2 Uniform layer model. We fitted the experimental NR data obtained at ILL by using the uniform layer model of the Si/SiO$_2$/initiator/solvent system described in subsection 5.1.2, augmented with one additional uniform layer to represent the polymer brush. Since the polymer brush undergoes large conformational changes between the two temperatures investigated, fits at the two temperatures were made separately; however, the volume of the polymer in the polymer layer was kept constant. To account for the gradual decrease of the polymer volume fraction at the outer edge of the brush, non-zero values of the roughness parameter were allowed. Hence, five independent parameters were used to describe the polymer brush: six parameters (polymer volume fraction in the polymer layer, thickness of the polymer layer, and the roughness of the polymer/solvent interface, all at the two temperatures) and one polymer volume constraint.

Fig. 6 shows that this approach enabled satisfactory agreement between the experimental (circles) and model (dashed curves) reflectivity. First, the thickness of the polymer layer at the higher temperature was determined accurately by using the positions of the fringes occurring at low q in cmSi; see also the inset in Fig. 6.

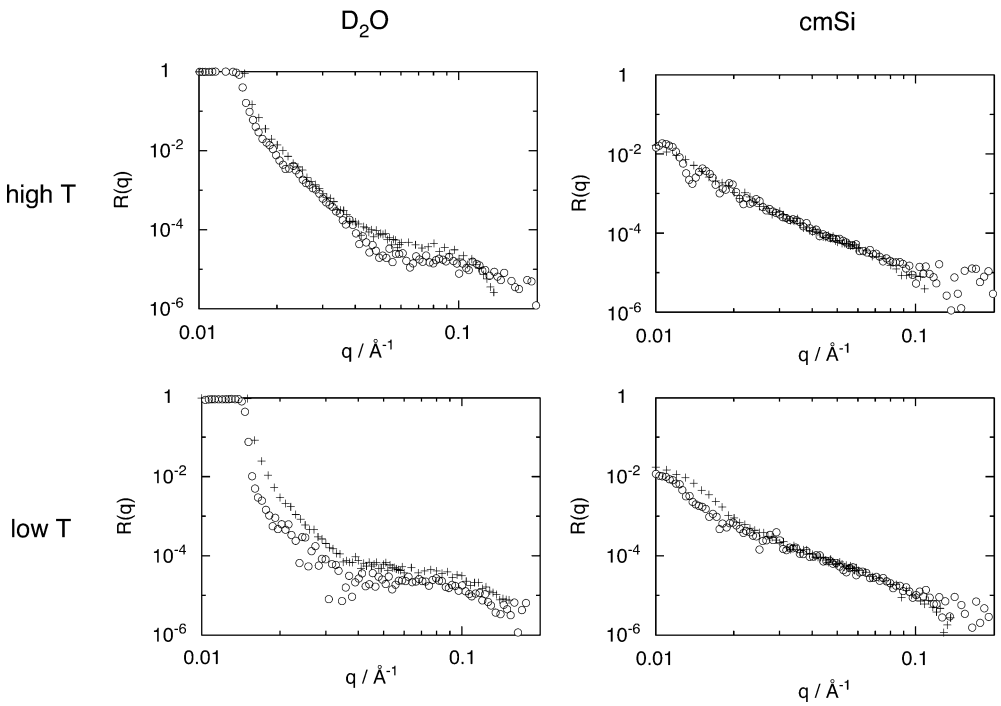

Fig. 5 Experimental reflectivity profiles obtained at NCNR (plus signs) and ILL (circles) at high temperature (top; 330 K at NCNR and 328 K at ILL) and low temperature (bottom; 300 K at NCNR and 293 K at ILL) in D_2O (left) and cmSi (right).

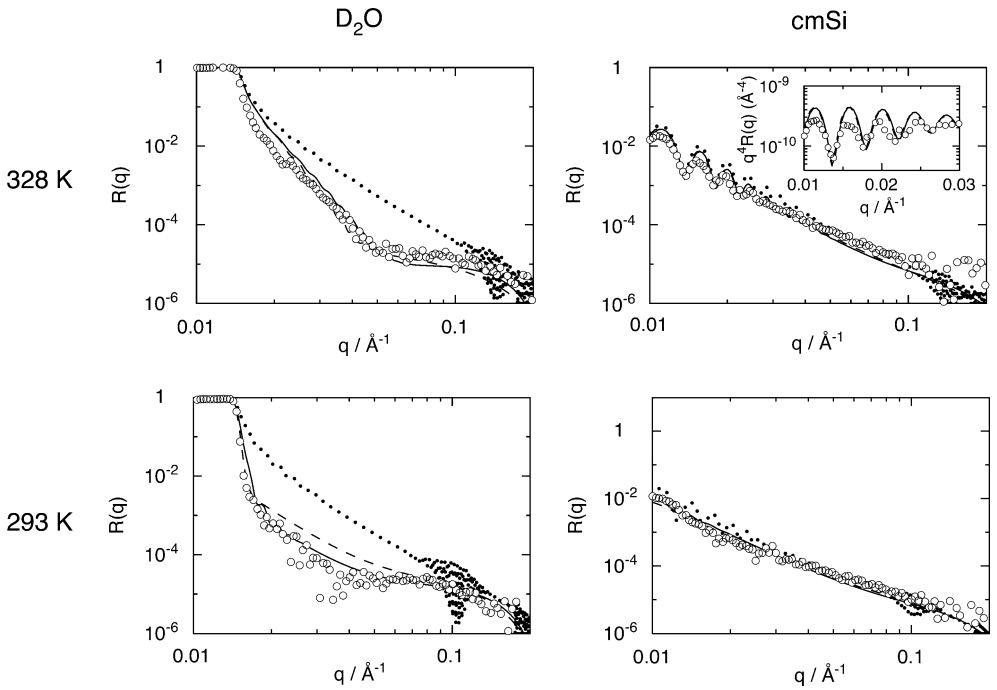

Fig. 6 Experimental reflectivity profiles obtained at ILL (circles) and fitted reflectivity profiles using a polymer layer model (dashed curves) and a lattice mean-field theory (solid curves) for polymers grafted on a Si/SiO_2/initiator surface at 328 K (top) and 293 K (bottom) in D_2O (left) and cmSi (right). Reflectivity profiles using a polymer layer model with zero roughness are also shown (dotted curves). The top right panel contains an inset displaying $q^4R(q)$ *versus* q for small q.

Second, the roughness at the higher temperature was fitted using the amplitude of reflectivity in D_2O at intermediate q-values. Thereafter, the polymer volume fraction was fitted to provide optimal representation of the reflectivity data in the two solvents. At the lower temperature, first the roughness was adjusted to suppress the fringes in the fitted reflectivity data. At that roughness, the amplitude of the reflectivity in D_2O became insensitive to the roughness, so only a lower limit of the roughness could be assessed. The thickness of the polymer layer and the polymer volume fraction of the polymer layer, with their product constrained, were then adjusted to provide optimal representation of the experimental data. This fitting protocol accounts for the different features of the reflectivity curves and provides an overall balanced fit. Table 4 provides the parameter values used to model the reflectivity curves. At the higher temperature, the polymer volume fraction increased from 55% to 75% and the thickness of the polymer layer decreased from 2200 to 1600 Å, which is consistent with the notion of a collapse of the polymer brush.

Table 4 Volume fractions (ϕ_i), thicknesses (l_i), and roughnesses (δ_i) of the uniform layer model for polymer-containing systems[a]

Layer	ϕ_i	l_i/Å	δ_i/Å
Si	1	Semi-infinite	0
SiO_2	1	9	0
Initiator	0.85 ± 0.05^{b}	30	0
Polymer (328 K)	$0.75 \pm 0.05^{b,c}$	$1600 \pm 50^{b,c}$	50 ± 5^{b}
Polymer (293 K)	$0.55 \pm 0.05^{b,c}$	$2200 \pm 50^{b,c}$	$250^{b,d}$

[a] The scattering length density of a layer was evaluated according to eqn (1). [b] Fitted. [c] The volume of the polymer given by the product of the polymer volume fraction and the thickness of the polymer layer was constrained to the same value at the two temperatures. [d] Only a lower limit could be determined; see text.

The model reflectivity curves obtained by using the layer model with zero roughness are also shown in Fig. 6 (dotted curves). It is clear that the non-zero roughness has a decisive influence on the amplitude of the reflectivity in D_2O, whereas the effect in cmSi is mainly to modulate the amplitude of the fringes. Thus, a layer model without Gaussian roughness or some other gradient in density does not provide a satisfactory fit.

5.2.3 Lattice mean-field model. The experimental NR data were also analyzed using a combination of the layer model and polymer segment density profiles. The refractive index and thickness of the silicon oxide and initiator layers, as discussed above, where used; however, the volume fraction profiles such as those shown in Fig. 3 were used to represent the distribution of polymer segments in the brush. Finally, the lattice size length d and the surface grafting density σ were used as fitting parameters. We recall that the former converts the lattice length to real units and the latter one is unknown and determined by the experiment and data fitting.

Fig. 6 (solid curves) shows the NR profiles predicted by the lattice mean-field polymer model. The value of the lattice size length d was first and uniquely determined by using the position of the fringes appearing in cmSi at the higher temperature (see also the inset of Fig. 6). Thereafter the grafting density σ was adjusted to provide the best overall representation for the four conditions. It is striking that the overall representation of the experimental NR data achieved by our lattice mean-field approach is even better than the fit obtained by the conventional uniform layer model. In particular, a significant improvement is

Table 5 Other parameters of the lattice mean-field model

Parameter	Value
Surface interaction	$kT\chi_{surface,water} = kT\chi_{surface,polymer(polar)} = 3$ kJ mol^{-1}
	$kT\chi_{surface,polymer(nonpolar)} = 0$ kJ mol^{-1}
Number of segments	$r_{polymer} = 1000$
Grafting density[a]	$\sigma = 0.08 \pm 0.005$
Length of lattice site[a]	$d = 14.7 \pm 0.3$ Å
Initiator volume fraction[a]	$\phi_{initiator} = 0.85 \pm 0.05$

[a] Fitted.

found in D_2O at $T = 293$ K. The values obtained for d and σ, given in Table 5, are very reasonable. A lattice size length of $d = 14.7$ Å compares well with the length of a few monomers and the grafting density $\sigma = 0.08$ together with $d = 14.7$ Å implies a spacing of about 50 Å between neighbouring grafted polymers. Assuming that the density of amorphous NIPAAM is 1 g cm^{-3}, the surface excess becomes 13 mg m^{-2} for the lattice model and 12 mg m^{-2} for the single layer model. Finally, the fraction of initiatior yielding a chain is experimentally unknown. However, from the amount of initiator per unit area, leading to an estimated cross-section area of the initiator of *ca.* 100 Å^2, and the fitted values of σ and d, the initiator efficiency is estimated to a few percent.

The close agreement between the experimental NR data and those predicted by the lattice mean-field theory augmented with a polymer model containing internal degrees of freedom verifies the usefulness of this theory to describe thermoresponsive polymer brushes. This verification is important because most other theories that describe thermoresponsive polymer systems are based on χ parameters with an explicit and fitted temperature (and sometimes volume fraction) dependence, see, *e.g.*, ref. 44. Furthermore, our approach involves only two independent polymer brush parameters compared to the five required for the conventional uniform layer model. We note that in addition to these parameters characterizing the polymer brush, we also treated the initiator volume fraction of the initiator layer as a fitting parameter.

The predictive capacity of the lattice mean-field theory is demonstrated in Fig. 7, which shows the increase of the fringes at low q-values in cmSi at increasing temperature. At 293 K and 303 K, the two lowest temperatures, the amplitude of the fringes is small and the number of fringes is few. As the temperature is increased from 303 K to 313 K, there is a strong increase of the amplitude and the number of fringes. This increase continues at still higher temperature but the changes become less accentuated. Hence, this analysis suggests that the collapse of the thermosensitive polymer brush at increasing temperature could be examined in detail in cmSi solution.

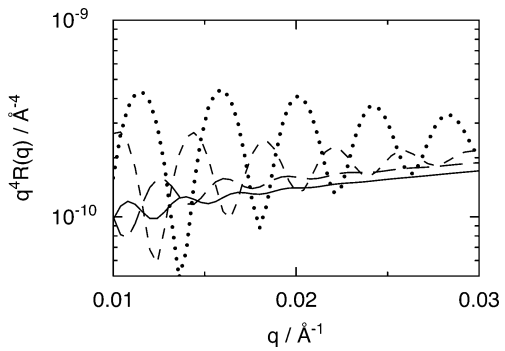

Fig. 7 Predicted reflectivity profiles $q^4R(q)$ *versus* q for small q obtained in cmSi at 293 K (solid curve), 303 K (long-dashed curve), 313 K (short-dashed curve), and 328 K (dotted curve) using the lattice mean-field theory. The reflectivity $R(q)$ at 293 K and 328 K are the same as in Fig. 6.

5.2.4 Comparison of the uniform layer and lattice mean-field models and appearance of fringes. The calculated reflectivity profiles are functions of the scattering length density profiles of the model systems. Fig. 8 displays the scattering length density profiles for the calculated reflectivity profiles given in Fig. 6. At the higher temperature the uniform layer and the lattice mean-field models produce nearly identical scattering length density profiles. The reasons behind the ability of the uniform layer model to describe the experimental system in this case are that the nearly constant polymer density throughout the collapsed polymer brush and that a Gaussian roughness model can account for the diffuse polymer/solvent interface. On the other hand, at the lower temperature the uniform layer model predicts systematically a higher reflectivity in the range 0.02 Å^{-1} < q < 0.07 Å^{-1}, which we attribute to the steep change of scattering length density at the edge of the polymer brush. An attempt to remedy the description for z < 2200 Å by increasing the roughness parameter and increasing the polymer volume fraction in the polymer layer does not improve the overall scattering length density profile, most likely due to a brush tail that becomes too long. Obviously, a uniform layer with a Gaussian roughness cannot describe the parabolic-like volume fraction profile with a short-range exponential tail as that shown in Fig. 3.

Fig. 6 showed that fringes appeared at the higher temperature in cmSi but not in D_2O. The reason for this difference can be found in Fig. 8. In cmSi the scattering length density of the two infinite media are the same, and hence the NR measurements explore the brush profile only. Since the brush profile has two sharp edges, fringes appear. On the other hand, in D_2O the scattering length densities of the brush and the substrate are similar. Here, NR probes essentially a single interface (the polymer–solvent interface); hence, no fringes appear.

6. Conclusion

Neutron reflectivity measurements at two different neutron sources have been performed on thermosensitive polymer brushes prepared with the same protocol. The neutron reflectivity data from the two experiments showed good agreement at two solvent contrasts and at two different temperatures.

A single uniform layer extended with roughness could represent the experimental reflectivity of the polymer brush, albeit different thicknesses and scattering lengths were needed for the different temperatures. Without roughness no reasonable representation could be obtained.

We have demonstrated a novel approach to evaluate experimentally obtained neutron reflectivity data for stimulus-responsive polymer brushes. In this approach, a physical model of the polymer brush is invoked to handle the temperature-dependent

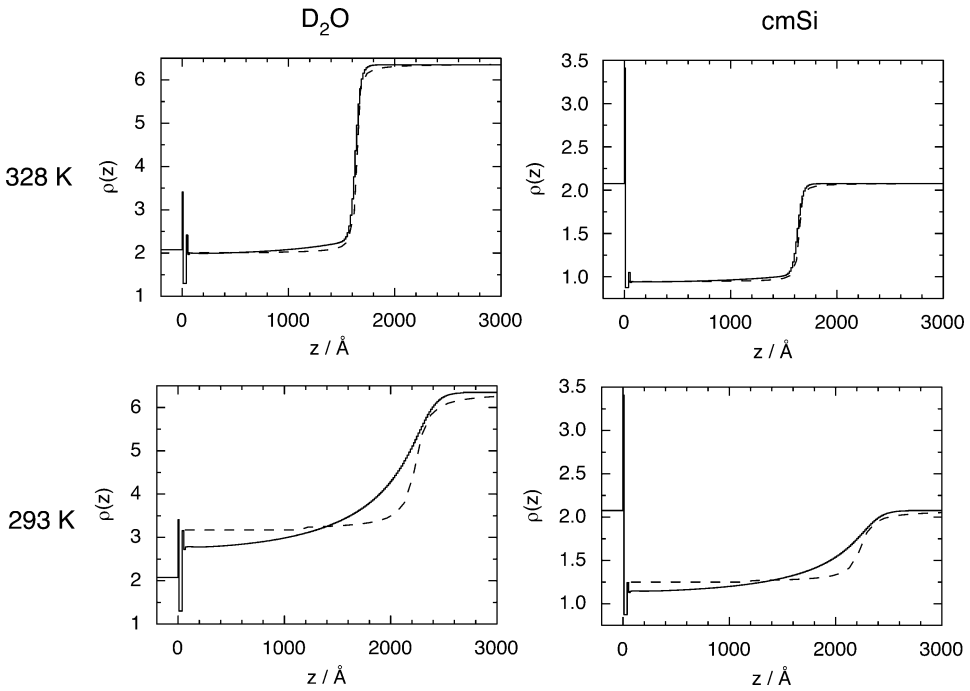

Fig. 8 Calculated scattering length density $\rho(z)$ *versus* distance z using the polymer layer model (dashed curves) and the lattice mean-field theory (solid curves) for polymers grafted on a Si/SiO_2/initiator surface at 328 K (top) and 293 K (bottom) in D_2O (left) and cmSi (right).

polymer–solvent interaction. These model calculations involve two sequential parts. First, model parameters describing the interaction in an aqueous polymer solution are determined by fitting predicted binodal curves to experimental phase behaviour. Second, the polymer brush density profiles to be used in the evaluation of the neutron reflectivity data are predicted. A central issue is that the *same* underlying model is used to evaluate the experimental data under the various experimental conditions involving different solvent contrasts and temperatures. Compared to the conventional layer approach, the new approach involves fewer fitting parameters. It is straightforward to extend the present approach to charge-containing polymers, including weak acids and bases, and to block copolymers as well as surfaces with an adsorbed polymer layer.

Finally, our approach suggests that one can model quantitatively, using relevant physical parameters, the outcome of NR experiments on polymer brushes. This information can be employed in the design of NR experiments to optimize the amount of information gained. For example, a suitable range and resolution of q as well as optimal brush heights and solvent contrasts could be determined. Here, we have demonstrated how the polymer model can be used to predict the expected reflectivity changes across the transition from an extended to collapsed polymer brush.

Acknowledgements

The authors are grateful for allocations of beam time at NCNR and ILL. We thank Sushil Satija for help with the experiments at NCNR and Giovanna Fragneto for help with experiments at ILL. Pauline Vandoolaeghe provided help with neutron reflectivity experiments and very useful discussions. Dr Marian Kaholek provided help in polymer brush synthesis. Financial support from the National Science Foundation (NSF) DMR-0502953 and the Swedish Foundation for Strategic Research (SSF) are gratefully acknowledged. The Swedish Research Council (VR) provided travel grants to assist with the experimental work.

References

1 N. Nath and A. Chilkoti, *Adv. Mater.*, 2002, **14**, 1243–1247.
2 J. Hyun, W. K. Lee, N. Nath, A. Chilkoti and S. Zauscher, *J. Am. Chem. Soc.*, 2004, **126**, 7330–7335.
3 N. I. Abu-Lail, M. Kaholek, B. LaMattina, R. L. Clark and S. Zauscher, *Sens. Actuators, B*, 2006, **114**, 371–378.
4 D. J. Beebe, J. S. Moore, Q. Yu, R. H. Liu, M. L. Kraft, B. H. Jo and C. Devadoss, *Proc. Natl. Acad. Sci. U. S. A.*, 2000, **97**, 13488–13493.
5 S. Balamurugan, S. Mendez, S. S. Balamurugan, M. J. O'Brien and G. P. Lopez, *Langmuir*, 2003, **19**, 2545–2549.
6 D. Goodman, J. N. Kizhakkedathu and D. E. Brooks, *Langmuir*, 2004, **20**, 2333–2340.
7 D. Goodman, J. N. Kizhakkedathu and D. E. Brooks, *Langmuir*, 2004, **20**, 6238–6245.
8 D. Goodman, J. N. Kizhakkedathu and D. E. Brooks, *Langmuir*, 2004, **20**, 3297–3303.
9 D. M. Jones, J. R. Smith, W. T. S. Huck and C. Alexander, *Adv. Mater.*, 2002, **14**, 1130–1134.
10 S. Kiodaki, S. Ohya, Y. Nakayama and T. Matsuda, *Langmuir*, 2001, **17**, 2402–2407.
11 W. Zhang, S. Zou, C. Wang and X. Zhang, *J. Phys. Chem. B*, 2000, **104**, 10258–10264.
12 M. Kaholek, W. K. Lee, S. J. Ahn, H. W. Ma, K. C. Caster, B. LaMattina and S. Zauscher, *Chem. Mater.*, 2004, **16**, 3688–3696.
13 H. Yim, M. S. Kent, D. L. Huber, S. Satija, J. Majewski and G. S. Smith, *Macromolecules*, 2003, **36**, 5244–5251.
14 H. Yim, M. S. Kent, S. Mendez, S. S. Balamurugan, S. Balamurugan, G. P. Lopez and S. Satija, *Macromolecules*, 2004, **37**, 1994–1997.
15 H. Yim, M. S. Kent, S. Satija, S. Mendez, S. S. Balamurugan, S. Balamurugan and C. P. Lopez, *J. Polym. Sci., Part B: Polym. Phys.*, 2004, **42**, 3302–3310.
16 G. Zhang, *Macromolecules*, 2004, **37**, 6553–6557.

17 T. Serizawa, D. Matsukuma, K. Nanameki, M. Uemura, F. Kurusu and M. Akashi, *Macromolecules*, 2004, **37**, 6531–6536.
18 M. A. Plunkett, Z. H. Wang, M. W. Rutland and D. Johannsmann, *Langmuir*, 2003, **19**, 6837–6844.
19 M. Kaholek, W.-K. Lee, B. LaMattina, K. C. Caster and S. Zauscher, in *Polymer Brushes: From Synthesis to Functional Microstructures*, ed. W. J. Brittain, R. C. Advincula, J. Ruhe and K. C. Caster, John Wiley & Sons, New York, 2004, pp. 381–402.
20 X. H. Wang, X. P. Qiu and C. Wu, *Macromolecules*, 1998, **31**, 2972–2976.
21 X. H. Wang and C. Wu, *Macromolecules*, 1999, **32**, 4299–4301.
22 T. P. Russell, *Annu. Rev. Mater. Sci.*, 1991, **21**, 249–268.
23 J. Penfold, R. M. Richardson, A. Zarbakhsh, J. R. P. Webster, D. G. Bucknall, A. R. Rennie, R. A. L. Jones, T. Cosgrove, R. K. Thomas, J. S. Higgins, P. D. I. Fletcher, E. Dickinson, S. J. Roser, I. A. McLure, A. R. Hillman, R. W. Richards, E. J. Staples, A. N. Burgess, E. A. Simister and J. W. White, *J. Chem. Soc., Faraday Trans.*, 1997, **93**, 3899–3917.
24 J. R. Lu and R. K. Thomas, *J. Chem. Soc., Faraday Trans.*, 1998, **94**, 995.
25 G. S. Smith, C. Toprakcioglu, S. M. Baker, J. B. Field, L. Dai, G. Hadziioannou, W. Hamilton and S. Wages, *Il Nuovo Cimento D*, 1994, **16**, 721–726.
26 F. T. Kiff, R. W. Richards, H. L. Thompson, D. G. Bucknall and J. R. P. Webster, *J. Phys. II*, 1997, **7**, 1871–1891.
27 I. Hopkinson, F. T. Kiff, R. W. Richards, D. G. Bucknall and A. S. Clough, *Polymer*, 1997, **38**, 87–98.
28 M. Sferrazza, R. A. L. Jones and D. G. Bucknall, *Phys. Rev. E*, 1999, **59**, 4434–4440.
29 K. Matyjaszewski and J. Xia, *Chem. Rev.*, 2001, **101**, 2921–2990.
30 V. F. Sears, *Neutron News*, 1992, **1992**, 26–27.
31 H. Rauch and W. Waschkowski, *Landolt-Boernstein 16A*, Springer, Berlin, 2000, ch. 6.
32 C. F. Majkrzak, S. K. Satija, N. F. Berk, S. K. Krueger, J. A. Borchers, J. A. Dura, R. Ivkov and K. O'Donovan, *Neutron News*, 2001, **12**, 25–29.
33 R. Cubitt and G. Fragneto, *Appl. Phys. A: Mater. Sci. Process.*, 2002, **74**, S329–S331.
34 P. J. Flory, *Principles of polymer chemistry*, Cornell University Press, Ithaca, Ithaca, NY, 1953.
35 G. Karlström, *J. Phys. Chem.*, 1985, **89**, 4962–4964.
36 M. Malmsten, P. Linse and K. W. Zhang, *Macromolecules*, 1993, **26**, 2905–2910.
37 J. M. H. M. Scheutjens and G. J. Fleer, *J. Phys. Chem.*, 1979, **83**, 1619–1635.
38 G. J. Fleer, M. A. Cohen Stuart, J. M. H. M. Scheutjens, T. Cosgrove and B. Vincent, *Polymers at interfaces*, Chapman & Hall, London, 1993.
39 P. Linse and M. Björling, *Macromolecules*, 1991, **24**, 6700–6711.
40 P. Linse and T. A. Hatton, *Langmuir*, 1997, **13**, 4066–4078.
41 J. E. Dennis Jr. and R. B. Schnabel, *Numerical methods for unconstrained optimization and nonlinear equations*, Prentice-Hall, Englewood Cliffs, 1983.
42 M. Born and E. Wolf, *Principles of Optics*, Cambridge University Press, Cambridge, 6th edn, 1980.
43 S. Lecuyer, G. Fragneto and T. Charitat, *Eur. Phys. J. E*, 2006, **21**, 153–159.
44 V. A. Baulin and A. Halperin, *Macromol. Theory Simul.*, 2003, **12**, 549–559.